ELSEVIER

NeuroImage

www.elsevier.com/locate/ynimg
NeuroImage 25 (2005) 1100–1111

An arteriolar compliance model of the cerebral blood flow response to neural stimulus

Yashar Behzadi[a,b] and Thomas T. Liu[a,*]

[a]*Center for Functional Magnetic Resonance Imaging and Department of Radiology, 9500 Gilman Drive, MC 0677, La Jolla, CA 92093-0677, USA*
[b]*Department of Bioengineering, University of California San Diego, La Jolla, CA 92037, USA*

Received 19 July 2004; revised 9 November 2004; accepted 7 December 2004
Available online 25 February 2005

Although functional magnetic resonance imaging (fMRI) is a widely used and powerful tool for studying brain function, the quantitative interpretation of fMRI measurements for basic neuroscience and clinical studies can be complicated by inter-subject and inter-session variability arising from modulation of the baseline vascular state by disease, aging, diet, and pharmacological agents. In particular, recent studies have shown that the temporal dynamics of the cerebral blood flow (CBF) and the blood oxygenation level dependent (BOLD) responses to stimulus are modulated by changes in baseline CBF induced by various vasoactive agents and by decreases in vascular compliance associated with aging. These effects are not readily explained using current models of the CBF and BOLD responses. We present here a second-order nonlinear feedback model of the evoked CBF response in which neural activity modulates the compliance of arteriolar smooth muscle. Within this model framework, the baseline vascular state affects the dynamic response by changing the relative contributions of an active smooth muscle component and a passive connective tissue component to the overall vessel compliance. Baseline dependencies of the BOLD signal are studied by coupling the arteriolar compliance model with a previously described balloon model of the venous compartment. Numerical simulations show that the proposed model describes to first order the observed dependence of CBF and BOLD responses on the baseline vascular state.

Keywords: Cerebral blood flow; BOLD responses; Arteriolar compliance model

Introduction

The blood oxygenation level dependent (BOLD) signal used in most fMRI experiments reflects local changes in deoxyhemoglobin content, and is a complex function of dynamic changes in cerebral blood flow (CBF), cerebral blood volume (CBV), and the cerebral metabolic rate of oxygen ($CMRO_2$) (Buxton et al., 1998b). Although significant progress has been made in characterizing and modeling the hemodynamic response (HDR) to brain activation (Buxton et al., 1998b; Hoge et al., 1999; Logothetis and Wandell, 2004; Mandeville et al., 1999), the quantitative interpretation of fMRI measurements is complicated by inter-subject and inter-session variability caused by differences in baseline physiology. An understanding of this dependency is especially relevant to the application of fMRI in clinical settings where significant variations in vascular state due to factors such as aging, disease, medication, or diet can confound the interpretation of the data (D'Esposito et al., 2003; Handwerker et al., 2004).

A number of recent studies have shown that the dynamic CBF response to neural stimulus exhibits an intriguing dependence on the baseline CBF level. Laser Doppler flow measurements characterizing the dynamic CBF response in rats indicate that the response slows down significantly with elevated baseline CBF due to hypercapnia (Ances et al., 2001; Bakalova et al., 2001; Matsuura et al., 2000a) and speeds up slightly with decreased baseline CBF due to either hypocapnia (Matsuura et al., 2000a) or hyperoxia (Matsuura et al., 2000b, 2001). An arterial spin labeling MRI study in rats has reported similar results (Silva et al., 1999). In humans, a hypocapnia-induced decrease in the rise time of the velocity response to visual stimulation has been observed in an ultrasound Doppler study of the posterior cerebral artery (Rosengarten et al., 2003). Additional evidence for a change in CBF dynamics can be inferred from BOLD measurements. Studies in visual cortex have shown that the temporal width and time to peak of the visual BOLD response increases with hypercapnia and decreases with hypocapnia, while the peak amplitude of the response show the opposite dependence (Cohen et al., 2002; Kemna and Posse, 2001). In addition, the post-stimulus undershoot in the response resolved more quickly with hypocapnia and appeared to be abolished with hypercapnia (Cohen et al., 2002). Cohen et al. (2002) note that the observed changes are perplexing, since a decrease in baseline CBF might be expected to correspond to reduced blood velocities and therefore a slower dynamic response (see for example, simulations

* Corresponding author. Fax: +1 858 822 0605.
E-mail address: ttliu@ucsd.edu (T.T. Liu).
Available online on ScienceDirect (www.sciencedirect.com).

1053-8119/$ - see front matter © 2005 Elsevier Inc. All rights reserved.
doi:10.1016/j.neuroimage.2004.12.057

in Mildner et al., 2001). The effect of hyperoxia on the BOLD response appears to be similar to the effect of hypocapnia and is consistent with laser Doppler flow findings in rats (Kashikura et al., 2001).

There is also growing evidence to suggest that the dynamics of the HDR change with age. Some studies of the dynamic BOLD response have described age-related increases in the temporal parameters (e.g., latency, time to peak) of the response (Mehagnoul-Schipper et al., 2002; Richter and Richter, 2003; Taoka et al., 1998). However, other studies have reported no changes with age (Buckner et al., 2000; D'Esposito et al., 1999). The reports of increases in the temporal parameters are consistent with the results of a functional near-infrared spectroscopy (fNIRS) study showing broadening and less undershoot in the time courses of oxyHB and deoxyHB in prefrontal cortex for the elderly subjects as compared to young subjects (Schroeter et al., 2003). Similarly, an ultrasound Doppler study of velocity increases in the posterior cerebral artery induced by visual stimulation found significant age-related decreases in the slopes of the velocity response (Panczel et al., 1999). The slowing down of the vascular dynamics may be related to the age-related reduction in the elasticity of the arteriolar wall, which reflects a decrease in smooth muscle and elastin components and an increase in the less distensible collagen and basement membrane components (Hajdu et al., 1990; Riddle et al., 2003). In addition, the decrease in baseline CBF with age may play a role (Bentourkia et al., 2000; Leenders et al., 1990; Marchal et al., 1992; Martin et al., 1991). The studies described suggest the following working observations: baseline CBF decreases with age, vascular compliance decreases with age, and the HDR decreases in amplitude and slows down with age. Note that in marked contrast to the quickening of the HDR with baseline CBF decreases induced by vasoconstrictive agents, the age-related decrease in baseline CBF is associated with a slowing down of the HDR.

As the field of fMRI has evolved, several dynamic models of the HDR have been developed. Two popular models, the *balloon model* and the *post-arteriole windkessel model*, were motivated in part by observations of a post-stimulus undershoot in the BOLD response and of differences between the CBF and CBV dynamic responses (Buxton et al., 1998b; Mandeville et al., 1999). In these models, CBF is the input that drives changes in CBV. To calculate the BOLD response, the balloon model is coupled to a dynamic model of the total amount of deoxyhemoglobin that reflects mass conservation and the relation between $CMRO_2$ and CBF (Buxton et al., 1998b).

To generate a CBF response that could be used as an input to the balloon model, Friston et al. (2000) introduced a linear feedback model of the CBF response. In this model, an increase in neural activity $u(t)$ (equal to zero at rest) leads to an increase in the concentration of a flow-inducing signal s through the first order differential equation $\dot{s} = \varepsilon u(t) - k_s s - g_f(f - 1)$, where ε is the neuronal efficacy, k_s is the rate constant for signal decay, and g_f is the gain constant for an auto-regulatory feedback term that drives the CBF back to its baseline value. The flow-inducing signal then leads to an increase in CBF through the relation $\dot{f} = s$ where f denotes CBF normalized by its baseline value. The form of the model was motivated by observations of an approximate linearity of the CBF response to stimulus (Miller et al., 2001), reports of post undershoots in CBF responses (Irikura et al., 1994), and the existence of vasomotion with a period of about 10 s (Mayhew et al., 1996). The two first-order equations may be combined to yield the overall second-order equation for flow $\ddot{f} + k_s\dot{f} + g_f(f - 1) = \varepsilon u(t)$. The properties of the equation can be understood by considering the impulse response $f_\delta(t) = 1 + \frac{\varepsilon}{\omega_0}\exp(-k_s t/2)\sin\omega_0 t$ where $\omega_0 = \sqrt{g_f - k_s^2/4}$ is the resonant frequency. As the impulse response is a constant term plus a damped sinusoid, the speed of the response depends on the resonant frequency. In order for the baseline CBF level to speed up the impulse response in this model, the primary effect of a decrease in CBF must be to increase the resonant frequency, either through decreasing the decay constant k_s or increasing the feedback gain constant g_f. Within the framework of the model, however, there is not a clear link between the values of the decay and gain constants and the baseline vascular state.

In this paper, we present an extension of Friston's model that explicitly models the contribution of the baseline vascular state to the dynamic CBF response. We refer to the modified model as the *arteriolar compliance model* because it models the link between neural activity and changes in the compliance of the arterioles. The motivation and basic form of the model are presented in the Theory section. Numerical simulations are then used to demonstrate the predictive capabilities of the model.

Theory

Nonlinear dependence of radius on compliance

The arteriolar compliance model is based on the following simplified picture. An arteriole experiences both intravascular pressure from the flowing blood and extravascular forces from the surrounding tissue and extracellular fluid. The intravascular and extravascular forces are balanced by circumferential stresses within the arteriole wall. There is an active stress component due to the vascular smooth muscle and a passive stress component due to connective tissues. The active and passive components act as two springs in parallel and together determine the overall compliance of the arteriole. With the assumption of constant external forces, the radius of the arteriole increases with its overall compliance. By analogy with a spring, the more compliant the arteriole, the more the vessel wall can stretch under a constant force.

Over the operating range of the arteriole, the relative contributions of the active and passive components to the overall compliance vary. Near or below the normal operating radius of the arteriole, most of the total stress is taken up by the muscle, so that the muscle compliance determines the overall compliance. As the radius saturates towards its maximum value, the muscle stress decreases while the passive stress increases exponentially (Davis and Gore, 1989; Lash et al., 1991). At these larger radii, most of the stress is taken up by the passive component, which then determines the overall compliance. Thus, there is a nonlinear dependence of total compliance on muscular compliance. This results in a nonlinear dependence of radius on muscular compliance that plays a critical part in explaining the dependence of the CBF dynamics on baseline CBF. Examples of the relations between stress, compliance and radius are shown in Figs. 1a and b for a 35-μm radius arteriole where the fraction λ of the total stress at rest taken up by the passive component is

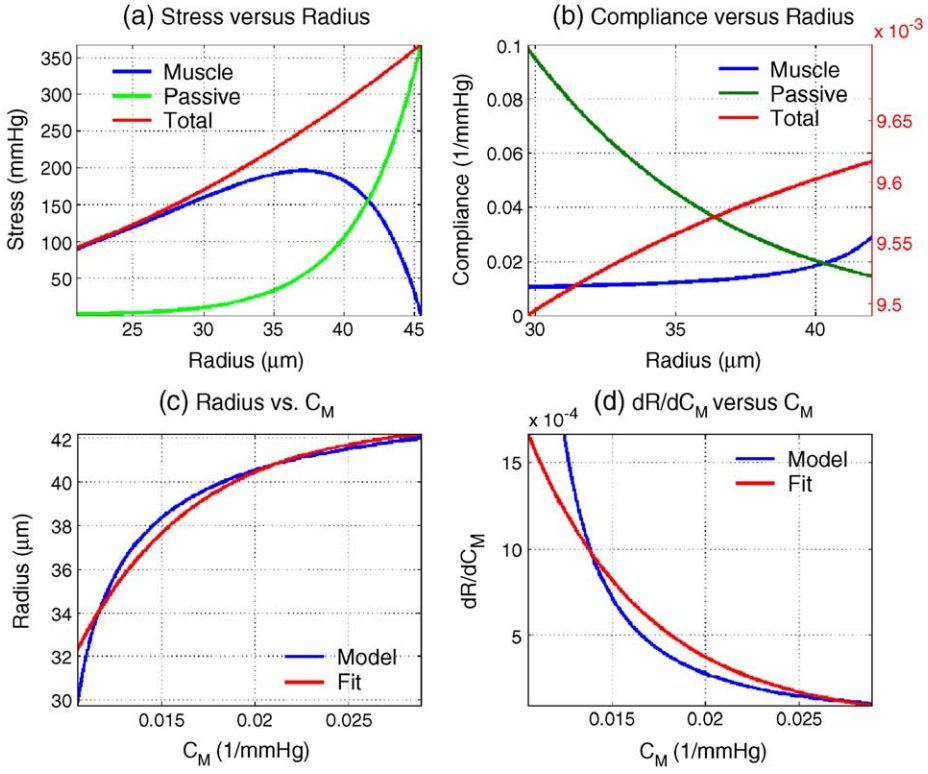

Fig. 1. Mechanical properties of the arteriole. (a,b) Muscle, passive, and total stress and compliance versus radius. In (b), the total compliance is the parallel combination of the passive and muscle compliances, with units labeled on the righthand side of the plot. (c) Radius versus compliance and exponential fit. (d) Derivative of radius with respect to compliance. Derivative of exponential fit is also shown.

equal to 0.15 and the maximum radius is 1.3 times the resting radius, consistent with typical values from Davis and Gore (1989) and Lash et al. (1991).

In Appendix A, we formalize the above arguments and derive an expression (Eq. (A10)) for the nonlinear relation between the arteriolar radius and smooth muscle compliance. An example of this relation is shown in Fig. 1c.

Link between neural activity and compliance

Although the precise mechanisms of neurovascular coupling are still poorly understood, it is generally thought that neural activity leads to an increase in the concentration of a number of vasoactive agents, such as nitric oxide, potassium ions, and adenosine (Attwell and Iadecola, 2002; D'Esposito et al., 2003; Iadecola, 2004). These agents affect muscular compliance by modulating the phosphorylation of myosin light chains (MLC) in the vascular smooth muscle cells (VSMC) either directly [e.g., through cyclic adenosine monophosphate (cAMP)] or through changes in the intracellular concentration of calcium (Davis and Hill, 1999; Murray, 1990; West et al., 2003). The kinetics of the pathway from neural activity to compliance are complex and still an area of active investigation, and so our approach is to construct the simplest model consistent with the experimental data. This is a second-order model consisting of a first stage relating neural activity to changes in a vasoactive signal and a second stage relating this signal to changes in muscular compliance.

The first stage approximates the complex path from neural activity to intermediate agents, such as nitric oxide and adenosine, onto final signaling agents, such as calcium, cAMP, cyclic guanine monophosphate (cGMP), and associated protein kinases (Davis and Hill, 1999; Murray, 1990; Somlyo and Somlyo, 1994; West et al., 2003). We lump the effects of the various vasodilatory and vasoconstrictive agents into a single vasoactive signal s, and adopt the first-order form of Friston's model to approximate the relation between neural activity and the change in the signal s as

$$\dot{s} = \varepsilon u(t) - k_s s - g_f(r^\gamma - 1) \quad (1)$$

with the flow feedback term rewritten in terms of the normalized radius $r = R/R_0$ where R_0 is the baseline radius and the exponent γ is 2 for plug flow and 4 for laminar flow. Blood flow in arterioles is well described by a laminar flow model, whereas blood flow in capillaries can vary between plug and laminar flow depending on the length of the vessel and the relative distribution and deformation of red blood cells (Fung, 1997). The feedback term models mechanisms that attempt to drive the system back to its baseline state, such as the action of stretch-mediated receptors in the vessel wall leading to an increase in the influx of calcium into the VSMC (Davis and Hill, 1999; Martinez-Lemus et al., 2003). It is important to note that, at rest, the vasoactive signal s is equal to zero, reflecting the balance between competing vasodilatory and vasoconstrictive signals. At the onset of activation, the concentration of vasodilatory agents (e.g., nitric oxide and cGMP) increases, leading to an increase in s. As the flow increases, the vasoconstrictive effects (e.g., influx of calcium) rise due to the feedback term and eventually balance the vasodilatory effects, so that s decreases. In the case of sustained activation, this leads to a new steady state with s again

equal to zero. Upon the cessation of activation, the vasoactive signal decreases, becoming initially negative as the vasodilatory effects decrease, before increasing back to zero when the vessel has returned to its baseline radius. Examples of these dynamics are shown in Fig. 2a.

In the second stage, an increase in s decreases the concentration of phosphorylated MLC, leading to a decrease in active muscle stress (Yang et al., 2003a) and hence an increase in muscle compliance. Approximating this with first-order kinetics yields the relation

$$\dot{c}_M = s \tag{2}$$

where $c_M = C_M/C_{M,0}$ denotes normalized compliance with baseline value $C_{M,0}$. Combining Eqs. (1) and (2) yields

$$\ddot{c}_M + k_s\dot{c}_M + g_f(r(c_M)^\gamma - 1) = \varepsilon u(t) \tag{3}$$

where the notation $r(c_M)$ indicates that normalized radius is a function of normalized muscle compliance.

Properties of the compliance model

The model presented above is clearly a simplified view of the underlying mechanisms. The question is whether such a simple model can explain the observed changes in the HDR with aging and induced changes in baseline CBF. Because of the nonlinear nature of the model, its properties are most readily explored using numerical simulations as described in the Methods section and the Results section. However, we can gain useful insight into the model dynamics by linearizing about the equilibrium point $c_M = 1$ (Wilson, 1999). To facilitate this process, we first approximate the nonlinear relation between radius and muscular compliance by the exponential function

$$R \approx R_{max}(1 - a_1\exp(-a_2C_M)) \tag{4}$$

where R_{max} is the maximum radius and a_1 and a_2 are constants obtained by fits to the nonlinear relation. An example of this approximation is shown in Fig. 1c. Substitution of this approximation into Eq. (3) yields the nonlinear second-order differential equation

$$\ddot{c}_M + k_s\dot{c}_M + g_f\left(\left(1 - a_1\exp\left(-a_2C_{M,0}c_M\right)\right)^\gamma R_{max}^\gamma/R_0^\gamma - 1\right) = \varepsilon u(t) \tag{5}$$

Linearization about the equilibrium point then leads to the second-order linear differential equation

$$\ddot{c}_M + k_s\dot{c}_M + \gamma g_f a_1 a_2 R_{max}R_0^{-1}C_{M,0}\exp\left(-a_2C_{M,0}\right)(c_M - 1) = \varepsilon u(t) \tag{6}$$

The effective feedback gain and impulse response associated with the linear equation are

$$g_{eff} = \gamma g_f a_1 a_2 R_{max}R_0^{-1}C_{M,0}\exp\left(-a_2C_{M,0}\right) \tag{7}$$

and

$$c_{M,\delta}(t) = 1 + \frac{\varepsilon}{\omega_{eff}}\exp(-k_st/2)\sin\omega_{eff}t \tag{8}$$

respectively, with resonant frequency $\omega_{eff} = \sqrt{g_{eff} - k_s^2/4}$. With hypocapnia, both R_0 and $C_{M,0}$ decrease with baseline CBF, so the feedback gain and resonant frequency increase as baseline CBF decreases. As a result, the linearized equation exhibits the property

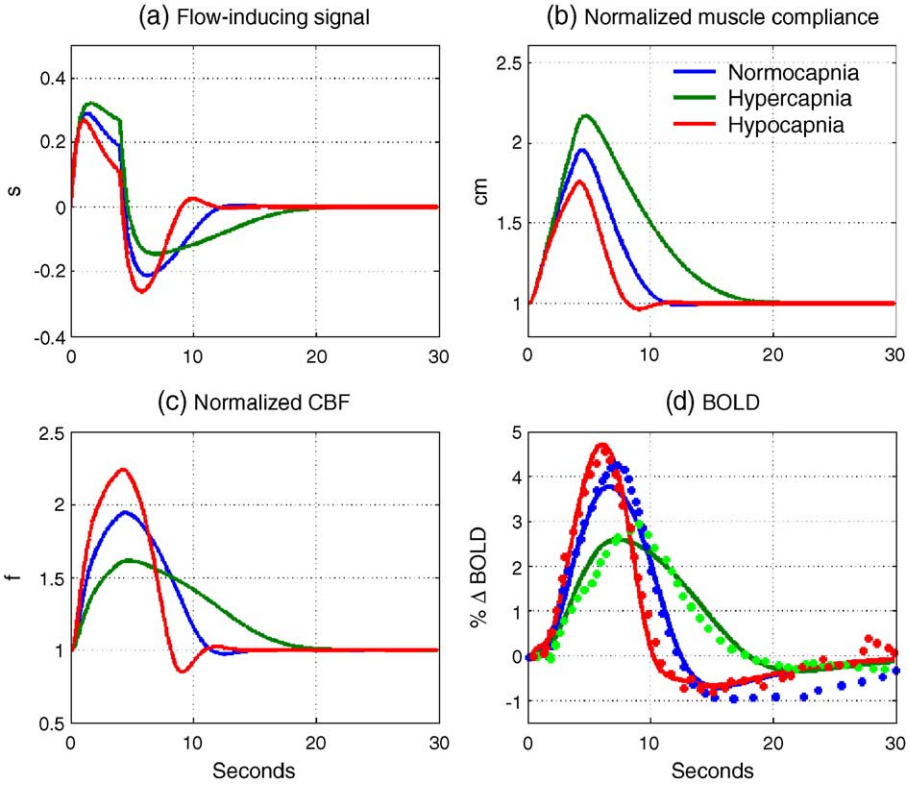

Fig. 2. Model responses under hypocapnic, normocapnic, and hypercapnic conditions. Data from Cohen et al. (2002) are shown by the plus symbols in panel (d).

that the dynamics of the impulse response speed up with a hypocapnia-induced decrease in baseline CBF. The importance of the nonlinear relation between radius and compliance can be appreciated by considering a linear relation of the form $R = b_1 C_M + b_2$. With the linear form, the effective gain is $g_{eff} = \gamma g_f b_1/(b_1 + b_2/C_{M,0})$, which decreases with lower values of baseline muscular compliance and CBF.

With age-related reductions in CBF and vascular compliance, the maximal radius R_{max}, initial radius R_0 and baseline total compliance all decrease, reflecting an increase in the passive stress fraction (Hajdu et al., 1990). With these changes, we find empirically that the constant terms a_1 and a_2 also decrease (e.g., calculations used for Fig. 3). This leads to a decrease in the feedback gain, because the term $a_1 a_2 R_{max} \exp(-a_2 C_{M,0})$ tends to decrease more quickly than the term $R_0^{-1} C_{M,0}$ increases.

The steady-state response of the compliance model can be obtained by setting the derivatives in Eq. (3) equal to zero and keeping in mind the saturation of the radius. The steady-state fractional change in CBF is then given by

$$f_{SS} - 1 = \begin{cases} \varepsilon u / g_f & \text{for } R_0\left(1 + \varepsilon u/g_f\right)^{1/\gamma} \le R_{max} \\ \left(R_{max}/R_0\right)^{\gamma} - 1 & \text{otherwise} \end{cases} \quad (9)$$

where the subscript SS denotes steady state. Thus, the model predicts that the fractional change in CBF is linearly related to the neural activity when the operating range of the vessel is such that its vessel radius is always less than the maximal radius. If the baseline CBF is greatly elevated, the fractional change in CBF can be limited by the inability of the arteriole to expand beyond its maximum radius.

Balloon model

The compliance model provides the link between neural activity and CBF. The BOLD response depends not only on dynamic changes in CBF but also on changes in cerebral blood volume (CBV) and the cerebral metabolic rate of oxygen ($CMRO_2$). We use the balloon model with viscoelastic terms to model the dynamic relation between CBF, CBV, and $CMRO_2$ and to determine the total volume of deoxyhemoglobin and its impact on the magnetic resonance signal (Buxton et al., 1998b; Obata et al., 2004). A summary of the form of the balloon model used in this paper is provided in Appendix B.

Methods

Modeling of carbon dioxide experiments

Numerical simulations were used to test the predictive capability of the compliance model. To demonstrate the effects of baseline CBF changes, we modeled the carbon dioxide experiments described in Cohen et al. (2002). The results of that study show good qualitative agreement with those of a similar human study by Kemna and Posse (2001) and an animal study by Matsuura et al. (2000a). We assumed normocapnic parameter values for baseline venous volume fraction, oxygen extraction fraction, and Grubb's law constant of $V_0 = 0.025$, $E_0 = 0.4$, and $\alpha = 0.38$, respectively (An and Lin, 2002; Grubb et al., 1974). The normocapnic transit time was calculated from the central volume principle, $\tau_0 = V_0/CBF$ (Stewart, 1894) assuming an average

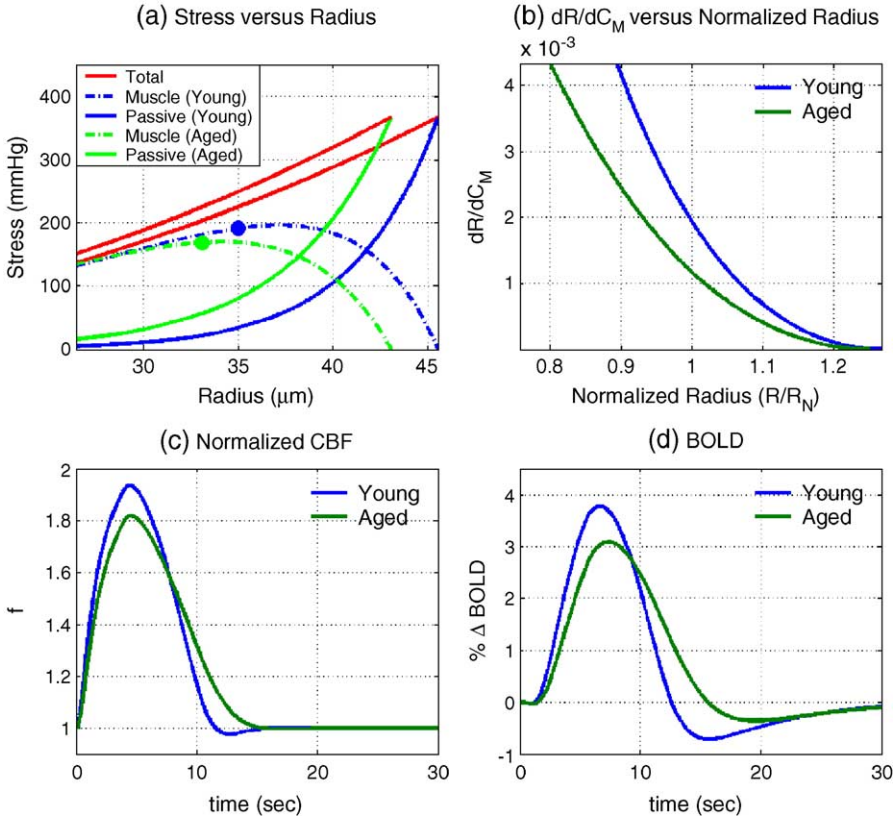

Fig. 3. (a) Stress versus radius for young and old subject. (b) dR/dC_M versus normalized radius. (c,d) Model CBF and BOLD responses.

baseline CBF of 60 ml/min-100 ml of tissue (equivalent to a flow rate of 0.01 s^{-1}) (An and Lin, 2002; Obata et al., 2004). The coupling constant (defined in Eq. (A14)) between the fractional change in CBF and the fractional change in $CMRO_2$ was assumed to be $n = 3$ across all levels of the partial pressure of carbon dioxide ($PaCO_2$) (Davis et al., 1998; Hoge et al., 1999; Kastrup et al., 2002). We also assumed that the baseline rate of oxygen metabolism $CMRO_{2,0}$ did not vary with $PaCO_2$ (Hoge et al., 1999). In addition, we assumed that the intravascular pressure, Grubb's law constant, and flow exponent ($\gamma = 4$ corresponding to laminar flow) did not vary across conditions (summarized in Table 1).

To determine the nonlinear relationship between arteriolar radius and the muscular compliance (Eq. (A10)), we assumed an intravascular pressure of 45 mm Hg with a normocapnic baseline arteriole radius and wall thickness of 35 and 7 μm, respectively (Fung, 1997). A reference radius, required for the definition of the circumferential strain, was selected to be half of the resting radius. The fraction λ of stress in the passive element at the resting radius was set to 0.15. It is important to note that in our model, we assume that the relation between radius and muscular compliance is determined by the normocapnic parameters, with changes in carbon dioxide level leading to different initial starting points on this operating curve.

Based on previous studies relating $PaCO_2$ to baseline CBF, the baseline CBF values under hypercapnia and hypocapnia were estimated to be 130% and 80%, respectively, of the normocapnic baseline value (Ito et al., 2003; Rostrup et al., 2002). For each level of $PaCO_2$, the following model parameters were adjusted from their normocapnic value to reflect the change in baseline CBF: initial radius R_0, initial wall thickness h_0, baseline blood volume fraction V_0, baseline oxygen extraction fraction E_0, baseline transit time τ_0, baseline muscular compliance $C_{M,0}$, and baseline total compliance $C_{TOT,0}$. The values of the adjusted parameters and details of the adjustment process are provided in Table 2. BOLD signal parameters for each $PaCO_2$ level were then determined from the adjusted values using equations presented in Appendix B.

Model simulations utilized the full form of the nonlinear relation between compliance and radius, as described by Eq. (A10). We constructed a lookup table to relate radius to compliance because of difficulty in inverting the closed form relation. The table was constructed with a radius step size of 0.01 μm and linear interpolation was used for values between steps. Simulation of the dynamic equations utilized a central Euler approximation of the coupled differential equations with a time step of 0.01 s. In fitting the model to the carbon dioxide data, the model parameters discussed above and summarized in Tables 1 and 2 were treated as constants, while the following parameters were treated as unknowns: neuronal efficacy ε, signal decay constant k_s, signal feedback constant g_f, normalized maximum radius $r_{max} = R_{max}/R_n$ where R_n is the normal operating radius corresponding to the normocapnic state, and viscoelastic time constants τ_+ and τ_-. The unknown parameters were constrained to be the same across the different carbon dioxide levels. Estimation of the unknown model parameters consisted of a two-step process. In the first step, model responses were generated over a coarse grid of parameter values with the range for each parameter shown in Table 3. The mean-squared error was then calculated between the data and the model responses, with the error at each level of $PaCO_2$ normalized by the power of the response. The parameter values that minimized the normalized mean-squared error summed over all levels were then used as initial estimates for the second step in which a constrained descent-based algorithm (fmincon function in MATLAB, Mathworks Inc., Natick, MA) was employed to obtain the final parameter estimates.

Table 1
Model parameters that were held constant across all model simulations

Parameter	Variable name	Value
Grubb's constant	α	0.38
$CMRO_2$ and CBF coupling constant	n	3
Flow exponent	γ	4
Intravascular pressure (mm Hg)	P_i	45

Table 2
Description of model parameters that were adjusted to reflect either carbon dioxide level-related or age-related changes in the normalized baseline cerebral blood flow $f_0 = CBF_0/CBF_{0,YN}$ where $CBF_{0,YN}$ denotes baseline CBF for normocapnia in the young state

Parameter	Normocapnia/ Young	Hypocapnia	Hypercapnia	Old
$CBF_0/CBF_{0,YN}$	1.0	0.8	1.3	0.8
R_0 (μm)	35.0	33.1	37.4	33.1
h_0 (μm)	7.0	7.33	6.62	6.62
λ	0.15	0.15	0.15	0.25
$C_{M,0}$ (1/mm Hg)	0.012	0.011	0.014	0.013
$C_{TOT,0}$ (1/mm Hg)	0.00956	0.00954	0.00958	0.00856
V_0	0.025	0.023	0.028	0.023
E_0	0.4	0.5	0.31	0.4
τ_0 (s)	2.5	2.87	2.13	2.87

Initial radius is $R_0 = R_{0,YN} f_0^{1/\gamma}$ where $R_{0,YN}$ is the initial radius for the young normocapnic state and $\gamma = 4$ for laminar flow. The initial wall thicknesses h_0 for the hypocapnic and hypercapnic states were computed using the incompressibility constraint in Eq. (A2), whereas the initial wall thickness for the old state was assumed to be 20% of R_0. The passive stress fraction λ at rest is used to generate the stress versus radius operating curves for the young and old states. It therefore corresponds to the stress fraction for the normocapnic condition in either the young or old state. Initial muscular compliance $C_{M,0}$ and total compliance $C_{TOT,0}$ for each state were calculated from Eqs. (A5) and (A10) with appropriate substitutions. The resting venous volume fraction V_0 was determined for each state with a Grubb's law relation $V_0 = (0.025) f_0^{\alpha}$. With the assumption of no change in baseline $CMRO_2$ between carbon dioxide levels, the resting oxygen fraction E_0 for each state is $E_0 = E_{0,YN}/f_0$ where $E_{0,YN}$ denotes the young normocapnic value. Reflecting the assumed decrease in $CMRO_2$ with age, the extraction fraction for the aged state is equal to that for the young normocapnic state. The resting transit delay τ_0 in each state reflects the central volume principle $\tau_0 = V_0/CBF_0$.

Modeling of aging effects

To model the effects of an age-related reduction in vascular compliance, we set the model parameters for the young response equal to those of the normocapnic condition described in the previous section. For the aged response, we assumed a decrease of 20% in the baseline CBF and increased the fraction λ of passive stress at rest from 0.15 to 0.25 of the total stress to reflect the reduction in the elasticity of the arteriolar wall resulting from the increase in the less distensible collagen and basement membrane components (Hajdu et al., 1990; Riddle et al., 2003). Initial radius R_0, baseline blood volume fraction V_0, and baseline transit time τ_0 were adjusted to reflect the change in baseline CBF as described in

Table 3
Model parameters that were estimated with a least squares fit to the data of Cohen et al. (2002)

Parameter	Variable name	Constrained range	Estimated value
Neuronal efficacy ($1/s^2$)	ε	0–1	0.57
Decay constant (1/s)	k_s	0–2	1.38
Feedback gain constant ($1/s^2$)	g_f	0–2	0.36
Viscoelastic time constant—inflation (s)	τ_+	0–30	0.17
Viscoelastic time constant—deflation (s)	τ_-	0–30	11.35
Maximum normalized radius	R_{max}/R_n	1.2–1.30	1.30

The maximum normalized radius is referenced to the normal operating radius R_n, which is defined as the normocapnic radius in either the young or old state. Details of the fitting process are described in the Methods section. Note that the simulations presented in Figs. 2 and 3 use the estimated values for all conditions (i.e., these model parameters do not vary across conditions).

Table 2. The baseline oxygen extraction fraction E_0 was held constant with age, consistent with studies showing that the baseline rate of oxygen metabolism $CMRO_{2,0}$ mirrors the age-related CBF decrease (Leenders et al., 1990; Pantano et al., 1984). The coupling constant between changes in CBF and $CMRO_2$ was assumed to be independent of age. The wall thickness was set to 20% of the resting radius, reflecting the assumption that the ratio of wall thickness to radius does not change with age. As shown in Fig. 3a, these parameter changes result in an upward and leftward shift of the total stress versus radius curve, as compared to the young curve. Reflecting this shift, the baseline total compliance $C_{TOT,0}$ exhibits an age-related decrease (see Table 2). The baseline muscular compliance $C_{M,0}$, however, shows an age-related increase since the muscle component accounts for a smaller fraction of the total stress in the aged state as compared to the young state. The model simulations for the aged state were performed using these adjusted parameters and the estimated model parameters obtained from the carbon dioxide data. In other words, it was assumed that the neuronal efficacy ε, signal decay constant k_s, signal feedback constant g_f, normalized maximum radius $r_{max} = R_{max}/R_n$ where the normal operating radius R_n is equal to the age-adjusted R_0, and viscoelastic time constants τ_+ and τ_- did not change with age.

Results

As shown in Fig. 2d, the simulated BOLD responses show good agreement with the data from the carbon dioxide experiments. Correlation of the model responses with the data yielded a correlation coefficient of 0.99. With hypercapnia the overall BOLD response is slowed, exhibiting an increase in the temporal width, a decrease in the peak amplitude, a reduction in the post-stimulus undershoot, and an increase in the rise time with respect to the normocapnic response. In contrast, hypocapnia leads to a decrease in the temporal width, an increase in the peak amplitude, and a decrease in the rise time. The model responses underestimate the amplitudes of both the peak of the response and the post-undershoot response for the normocapnic data. This partly reflects the fact that the viscoelastic time constants were maintained constant across conditions.

The compliance model parameters describing neuronal efficacy ε, signal decay constant k_s, and flow dependent feedback gain g_f were estimated to be 0.57 s^{-2}, 1.38 s^{-1}, and 0.36 s^{-2}, respectively. These values are similar to the corresponding average values of 0.54 s^{-2}, 0.65 s^{-1}, and 0.41 s^{-2} reported for the linear feedback model in Friston et al. (2000). The balloon model viscoelastic time constants were found to be 0.17 s during inflation and 11.35 s during deflation. The normalized maximum radius was estimated to be 1.30.

It is important to stress that the model responses were obtained with the signal decay and feedback gain parameters held constant across the levels of carbon dioxide. Thus, the speeding up or slowing down of the response was due primarily to the change in baseline compliance, which then modulates the effective feedback gain (see Theory section). This is in marked contrast with the linear feedback model, which, as discussed in the Introduction, requires a change in either the signal decay or feedback gain parameter in order to slow down or speed up the response in a manner consistent with the experimental data. In addition, although the parameters estimated for the compliance model show good agreement with those previously reported for the linear feedback model, these models are not equivalent, even for the normocapnic state. The feedback term in the compliance model exhibits a nonlinear and dynamic dependence on CBF, while the feedback term in the linear feedback model is assumed to be a constant.

A detailed examination of the various responses in Fig. 2 is useful for understanding the dependence on baseline CBF. As shown in Fig. 2a, the initial slopes of the vasoactive signal responses are independent of the baseline state, reflecting the fact that the signal decay and flow feedback terms in Eq. (1) are initially small so that the time derivative of the vasoactive signal is proportional to neural activity. Similarly, the initial slopes of the normalized muscle compliance curves are independent of the baseline state. In contrast, the slopes of the normalized CBF and BOLD responses in Figs. 2c and d, respectively, exhibit a baseline dependence that reflects the nonlinear relation between the radius and smooth muscle compliance described by Eq. (A10). To better understand this dependence, we consider the derivative dR/dC_M of radius with respect to muscular compliance. Due to the nonlinear relation between radius and compliance, this derivative also exhibits a nonlinear dependence on muscular compliance, as shown in Fig. 1d. At lower baseline muscular compliance values, corresponding to lower baseline CBF with hypocapnia, dR/dC_M is elevated with respect to the normocapnic condition. Conversely, at higher baseline muscular compliance values, corresponding to elevated baseline CBF with hypercapnia, dR/dC_M is reduced. As a result, the same fractional change in muscular compliance under hypocapnia will result in a larger fractional changes in radius and CBF as compared to the normocapnic condition, while under hypercapnia the percent CBF change is reduced.

After its initial rise, the vasoactive signal decreases more quickly under hypocapnia and more slowly under hypercapnia. In the hypocapnic condition, the increased fractional change in CBF leads to a larger flow dependent feedback term that drives the vasoactive signal back to zero more quickly. Referring back to the insight gained from the linearization analysis, we also note that the larger feedback term corresponds to a higher resonant frequency in the linearized form of the model. In contrast, the feedback term is

smaller under hypercapnia and the vasoactive signal moves more slowly toward the baseline value. Because of the slower decrease of the vasoactive signal, the normalized muscular compliance reaches a larger value in the hypercapnic condition as compared to the normocapnic and hypocapnic states. However, as shown by the curves in Fig. 2c, the greater percent change in compliance does not translate into a larger percent change in CBF. Instead, the hypercapnic response exhibits the smallest percent CBF increase, reflecting the lower value of dR/dC_M. The peak values of the normalized flow during normocapnia, hypocapnia, and hypercapnia are 1.95, 2.25, and 1.60, respectively. For comparison, we find from Eq. (9) that the normocapnic and hypocapnic normalized steady state flows are both given by $1 + \varepsilon u/g_f = 2.6$ (assuming a step input $u = 1$), while the hypercapnic steady-state response is given by $(R_{max}/R_0)^{\gamma} = 2.2$.

After the stimulus has ended, the vasoactive signal becomes negative, leading to a decrease in muscular compliance. Because of the larger flow feedback term, the hypocapnic vasoactive signal and compliance responses resolve the most quickly. This is also reflected in the CBF and BOLD responses. The simulated CBF responses under normocapnia and hypocapnia exhibit a post-stimulus undershoot that is not observed in the slower response under hypercapnia. The post-stimulus undershoot in the hypercapnic BOLD response is minimal, indicating a similarity between the time courses of the post-stimulus CBF and CBV responses (Buxton et al., 1998b; Mandeville et al., 1999). In contrast, the post-stimulus undershoots in the hypocapnic and normocapnic BOLD responses reflect the contributions of the CBF undershoots and the relative mismatch of the CBF and CBV responses.

The stress versus radius curves for young versus aged conditions are shown in Fig. 3a. The total stress is slightly increased in the aged condition, reflecting a reduction in the normal resting radius and wall thickness with intravascular pressure held constant between conditions. The passive stress curves exhibit an age-related shift similar to that described in Hajdu et al. (1990), with a smaller maximum radius and a larger fraction of passive stress in the aged state. The increased passive fraction makes the vessel less responsive to changes in muscular compliance. This is reflected in the curves of Fig. 3b showing a downward shift in the derivative dR/dC_M with aging. The age-related shift results in a smaller increase in radius and CBF for a given increase in muscular compliance. The smaller increase in CBF leads to a smaller flow-dependent feedback term and hence a slower response in the aged state. These effects are reflected in the CBF responses of Fig. 3c, with the aged response exhibiting a smaller amplitude and slower dynamics as compared to the young response. The BOLD response shown in Fig. 3d inherits these features. Additional numerical simulations (not shown) indicate that simply lowering baseline CBF without also increasing the passive stress fraction does not significantly slow down the responses, because this merely shifts the operating curve (stress vs. radius) of the arteriole as opposed to changing the shape of the curve. In addition, as described in the Methods section, the simulations were performed with the assumption that $CMRO_2$ decreases with age so that the baseline oxygen extraction fraction E_0 does not change with age. With the alternative assumption that $CMRO_2$ remains constant with age, E_0 would increase, and the amplitude of the aged BOLD response would be greater than that of the model response shown.

Discussion

We have presented a nonlinear dynamic model linking changes in neural activity to changes in arteriolar compliance and CBF. The compliance model may be considered an extension of the linear dynamic model proposed in Friston et al. (2000). In the present model, the vasoactive signal modulates arteriolar muscular compliance as opposed to directly modulating CBF as in the prior model. Changes in total arteriolar compliance then lead to changes in vessel radius and CBF. The total compliance is modeled as the parallel combination of an active component representing smooth muscle and a passive component representing connective tissue. This results in a nonlinear relation between radius and smooth muscle compliance. At smaller radii, the total compliance is determined primarily by the smooth muscle compliance, so that neurally induced changes in muscle compliance lead to relatively large changes in vessel radius. At larger radii, the total compliance is determined primarily by the passive component so that changes in muscle compliance are less effective at modulating the vessel radius.

Using numerical simulations, we have shown that the compliance model predicts to first order the observed changes in the temporal dynamics of the CBF and BOLD responses as a function of baseline CBF. The model also predicts the slowing down of the responses with age-related decreases in vascular compliance.

Although the compliance model in its present form provides relatively good fits to experimental observations, it is clearly a simplification of the underlying mechanisms. Further experimental and theoretical work is required to develop more accurate and complex models. For example, although the output of the compliance model is CBF, most of the currently available observations revealing baseline vascular effects use measurements of the BOLD response. This is in part because of the lower signal-to-noise ratios (SNR) exhibited by present methods for measuring CBF, as compared to methods for measuring BOLD. Detailed measurements of dynamic CBF responses as a function of baseline CBF would allow for a more direct validation of the compliance model. In addition, in vitro studies of isolated arterioles and in vivo studies of CBF responses in animals, using invasive methods that cannot be applied to humans, would be useful for more fully revealing the mechanisms underlying the effects of the baseline vascular state.

The current model employs a first stage linking neural activity to a vasoactive signal and a second stage linking to the vasoactive signal to changes in muscular compliance. Further development of the model would lead to more accurate descriptions of the pathways in each stage. For example, the first stage involves initial pathways from neural activity to intermediate vasoactive agents, such as nitric oxide, and secondary pathways from the intermediate agents to final signaling agents, such as calcium. Thus, the next level of model development could entail modeling the first stage as the cascade of two first order systems. A recently presented biophysical model linking calcium to muscular compliance (Yang et al., 2003a,b) may provide useful insights for modifying the second stage of the compliance model. This model integrates a large body of current knowledge about the electrochemistry and chemo-mechanics of the vascular smooth muscle cell, and has been shown to fit experimental measurements of the myogenic response in isolated cerebral arterioles. In its current state, the model is probably too complex (23 state variables and

roughly 50 assumed constants) to robustly model dynamic responses. However, numerical simulations of the biophysical model could be useful in exploring further developments of the second stage of the compliance model. For example, the present model might be expanded to incorporate a description of the phosphorylation of the myosin light chains.

While the compliance model is the primary focus of this paper, the balloon model plays an important role in testing the predictions of the compliance model with experimental BOLD observations. Although as discussed above, CBF measurements are preferable for direct validation of the compliance model, BOLD measurements are likely to play an important role in further development of the model, due to their better SNR and temporal resolution. In addition, the widespread use of BOLD measurements in fMRI studies makes it critical to understand the effect of the baseline vascular state on the BOLD responses. In the current form of the balloon model, we have assumed a tight coupling between CBF and $CMRO_2$ (Eq. (A14)) and also assumed that $CMRO_2$ does not change with carbon dioxide level. Recently, Zheng et al. (2002) have proposed a dynamic model that takes into account the modulatory effect of tissue oxygenation on the coupling between CBF and oxygen delivery. The model appears to yield a better prediction of the dynamic $CMRO_2$ response to neural stimulus and also provides a prediction of the observed $CMRO_2$ response in anesthetized rats to hypercapnia. The incorporation of the dynamic oxygen delivery model may therefore improve the predictive capability of the combined compliance and balloon model presented here. A reformulation of the viscoelastic properties of the balloon model may also lead to better predictions. In fitting the results of the carbon dioxide experiments, we found that it was difficult to simultaneously fit the post-stimulus undershoot of the BOLD response under all baseline conditions (see Fig. 2). A better fit may be achievable with a model that incorporates the effect of baseline CBV and venous compliance on the dynamics of the venous compartment.

In this paper, we have focused on the structure of the compliance model and its ability to predict the effect of the baseline vascular state on the hemodynamic response to stimulus. The estimation of model parameters was achieved using a two-step procedure consisting of a global minimization over a coarse grid followed by a conventional descent based algorithm. This approach may not be optimal from the point of view of computational efficiency or robustness. Friston (2002) and Friston et al. (2003) have applied a Bayesian identification scheme to the combination of the second-order linear feedback model (described in the Introduction) with the balloon model. This scheme utilizes the expectation-maximization algorithm for estimating the conditional or posterior distribution of the model parameters. The inclusion of priors in the estimation procedure enables robust and rapid convergence of the estimation process. In addition, the conditional densities provided by a Bayesian scheme enable inference about the dependencies between different model parameters. It is likely, therefore, that the application of a Bayesian scheme to the compliance model would improve the robustness of the estimation process and lead to a better understanding of the interdependence and relative importance of the different model parameters. Finally, an extension of the Bayesian framework to examine interactions among different brain regions has recently been presented in the form of dynamic causal models (Friston et al., 2003). Incorporation of the compliance model into the current dynamic causal model structure could prove useful in examining the effect of the baseline vascular state on the effective connectivity between brain areas.

Acknowledgments

This work was funded by a Biomedical Engineering Research Grant from the Whitaker Foundation. We thank Khaled Restom, Kamil Uludag, Matt Cronin, and Rick Buxton for helpful discussions.

Appendix A. Radius and muscular compliance

In this section, we show that there is a nonlinear relation between arteriolar radius and the compliance of the vascular smooth muscle. We begin with the force balance equation for a cylindrical thick walled vessel

$$RP_i - (R+h)P_e = (\sigma_M + \sigma_P + \sigma_V)h \tag{A1}$$

where P_i and P_e are the intravascular and extravascular pressures, respectively; σ_M, σ_P, and σ_V are muscular, passive, and viscoelastic stress terms, respectively; and h is the wall thickness (Ursino, 1991). We assume that the vessel wall is incompressible so that the wall thickness satisfies the constraint

$$h = -R + \sqrt{R^2 + 2R_0h_0 + h_0^2} \tag{A2}$$

where R_0 and h_0 are the initial values of the inner radius and wall thickness. With this relationship, the vessel wall gets thinner as the radius increases. To obtain a steady-state relation between compliance and radius, we may neglect the viscoelastic stress term, which is proportional to the rate of change of the radius. Because of the lack of data on the extravascular pressure exerted by the surrounding tissue, we neglect this term to simplify our presentation. Choosing a constant value for this term would not change the overall approximation that we derive.

With the above assumptions, the total stress can be expressed as

$$\sigma_{Tot} = \sigma_P + \sigma_M = \frac{P_i}{h}R. \tag{A3}$$

This is analogous to two springs acting in parallel in which the overall stress is the sum of the stresses in each individual element, and the individual strains are equal to the total strain. In contrast, two springs in series would experience equal stresses and the overall strain would be equal to the sum of the individual strains at each spring (Fung, 1994).

The total compliance of the arteriole is defined as

$$C_{Tot} = \frac{E_{Tot}}{\sigma_{Tot} - \sigma_{Tot,Ref}} \tag{A4}$$

where σ_{Tot} is defined as a function of radius in Eq. (A3), $\sigma_{Tot,Ref}$ is the stress at a reference radius R_{ref}, and the Lagrangian finite strain term is $E_{Tot} = (R^2/R_{ref}^2 - 1)/2$ (Fung, 1993). The reference radius is chosen to be smaller than the lowest radius of interest so that all stresses and strains are positive. Because the total stress is the sum of the passive and muscle stresses, the total compliance may also be expressed as the parallel combination

$$C_{Tot} = \frac{C_P C_M}{C_P + C_M} \tag{A5}$$

of a muscle compliance term C_M and passive compliance term C_P. These are defined as

$$C_M = \frac{E_{Tot}}{\sigma_M - \sigma_{M,ref}}, \quad C_P = \frac{E_{Tot}}{\sigma_P - \sigma_{P,ref}} \tag{A6}$$

where $\sigma_{M,Ref}$ and $\sigma_{P,Ref}$ are the respective stresses at the reference radius and $\sigma_{Tot,Ref} = \sigma_{P,Ref} + \sigma_{M,Ref}$. With these definitions and the relation in Eq. (A3), Eqs. (A4) and (A5) are mathematically equivalent. Note that in the parallel combination of compliances in Eq. (A5), the smaller compliance dominates the total compliance. This is analogous to the less compliant spring dominating the overall compliance when two springs are in parallel.

From Eqs. (A3) and (A6), we can express muscular compliance as a function of the vessel radius and passive stress

$$C_M = \frac{E_{Tot}}{P_i\left(\frac{R}{h} - \frac{R_{ref}}{h_{ref}}\right) - (\sigma_P - \sigma_{P,Ref})}. \tag{A7}$$

It has been shown that passive stress is well modeled as an exponential function of radius

$$\sigma_P = \sigma_{P,0}\exp(k_P R) \tag{A8}$$

where $\sigma_{P,0}$ and k_P are empirical constants (Fung, 1997). Estimation of these constants is based on the following observations: (a) the ratio of the stresses in the elastic and muscle elements as a function of radius is conserved across various orders of the arteriole tree; (b) at the normal operating point radius R_n, 80–90% of the total tension is within the muscle element; and (c) nearly all the stress is exerted by the passive element when the vessel is at its maximum radius R_{max} (Davis and Gore, 1989; Lash et al., 1991). Application of the boundary conditions at R_n and R_{max} in conjunction with Eq. (A3) for the total stress yields

$$\sigma_P = \frac{P_i \lambda R_n}{h_n}\left(\frac{R_{max} h_n}{\lambda R_n h_{max}}\right)^{\left(\frac{R-R_n}{R_{max}-R_n}\right)} \tag{A9}$$

where λ is the fraction of total stress in the passive element at R_n, and h_n and h_{max} are the vessel wall thickness at R_n and R_{max}, respectively. Substitution of Eq. (A9) into Eq. (A7) yields an expression for muscular compliance as a function of radius

$$C_M = \frac{\frac{1}{2}\left(\frac{R^2}{R_{ref}^2} - 1\right)}{P_i\left(\frac{R}{h} - \frac{R_{ref}}{h_{ref}}\right) - \frac{P_i \lambda R_n}{h_n}\left(\left(\frac{R_{max} h_n}{\lambda R_n h_{max}}\right)^{\left(\frac{R-R_n}{R_{max}-R_n}\right)} - \left(\frac{R_{max} h_n}{\lambda R_n h_{max}}\right)^{\left(\frac{R_{ref}-R_n}{R_{max}-R_n}\right)}\right)} \tag{A10}$$

Assuming an intravascular pressure of 45 mm Hg with a normal operating point radius and wall thickness of 35 and 7 μm, respectively, we use Eq. (A10) to plot the relation between radius and muscle compliance in Fig. 1c. Additionally, the reference radius was selected to be half of the resting radius with λ and R_{max}/R_n set to 0.15 and 1.3, respectively. This relation is fairly well approximated by the exponential form $R = R_{max}(1 - a_1 e^{-a_2 C_m})$, also shown in the Fig. 1c.

Appendix B. Balloon model

In the balloon model with viscoelastic effects, the venous compartment is treated as a distensible balloon (Buxton et al., 1998b). The flow into the balloon is determined by the compliance model, while the flow out of the balloon is modeled as

$$f_{out}(v) = v^{1/\alpha} + \tau_v \dot{v} \tag{A11}$$

where v denotes the venous volume normalized by its initial value, τ_v is the viscoelastic time constant (equal to τ_+ and τ_- during inflation and deflation, respectively), and α is an empirical constant that determines the steady-state power law relation between flow and volume (Buxton et al., 1998a; Grubb et al., 1974). The flow and volume dynamics follow the mass conservation relation

$$\tau_0 \dot{v} = f - f_{out}(v) \tag{A12}$$

where τ_0 is the mean transit time to traverse the venous compartment at rest.

The equation for mass conservation of deoxyhemoglobin in the balloon is

$$\tau_0 \dot{q} = f\frac{E(f, E_0)}{E_0} - f_{out}(v)\frac{q}{v} \tag{A13}$$

where q is the total deoxyhemoglobin content normalized by its initial value, E_0 is the net extraction fraction of oxygen at rest, and $E(f, E_0)$ is the extraction fraction as a function of flow and E_0. An expression for $E(f, E_0)$ is obtained by assuming a linear coupling

$$n = \frac{\Delta CBF/CBF_0}{\Delta CMRO_2/CMRO_{2,0}} = \frac{f-1}{m-1} \tag{A14}$$

between the fractional change in CBF and the fractional change in $CMRO_2$, where n is an empirical coupling constant and m is $CMRO_2$ normalized by its initial value (Buxton, 2002). The relation between CBF and $CMRO_2$ is $CMRO_2 = E \cdot C_A \cdot CBF$ where C_A is the arterial oxygen concentration. This may be written in normalized quantities as $E = E_0\, m/f$. Combining this expression with Eq. (A14) yields

$$E(f, E_0) = E_0\frac{f + n - 1}{nf} \tag{A15}$$

which permits us to rewrite Eq. (A13) as

$$\tau_0 \dot{q} = \frac{f + n - 1}{n} - f_{out}(v)\frac{q}{v} \tag{A16}$$

The BOLD signal change as a function of normalized volume and deoxyhemoglobin is

$$\Delta S/S_0 = V_0[(k_1 + k_2)(1 - q) - (k_2 + k_3)(1 - v)] \tag{A17}$$

where V_0 is the resting blood volume fraction (Obata et al., 2004). The first constant term $k_1 = 4.3 v_0 E_0 TE$ where TE is the echo time of the sequence and $v_0 = 40.3 \cdot (B_0/1.5)\ s^{-1}$ is a magnetic field (B_0) dependent frequency offset. The second constant term $k_2 = \beta r_0 E_0 TE$ where $\beta = S_E/S_I$ is the intrinsic ratio of blood to tissue signals at rest and r_0 is the slope of the intravascular relaxation rate $R_{2,I}^*$ versus the extraction fraction E (Li et al., 1998). The blood and tissue signals are defined as $S_E = S_{E,0}\exp(-TE/T_{2,E}^*)$ and $S_I = S_{I,0}\exp(-TE/T_{2,I}^*)$, respectively, where T_{2I}^* and T_{2E}^* are the resting intravascular and extravascular transverse relaxation times and S_{E0} and S_{EI} are the effective spin densities. For this paper, we assume average values of $T_{2,E}^* = 25$ ms and $T_{2,I}^* = 12.8$ ms at 7 T (Yacoub

et al., 2001) and also assume that the effective spin densities are equal. In vitro measurements have shown that r_0 exhibits a quadratic dependence on field strength (Silvennoinen et al., 2003), so that we may calculate its value as a function of field strength as $r_0 = 25.0 \cdot (B_0/1.5)^2$ where 25.0 s^{-1} is the measured in vivo value at 1.5 T (Li et al., 1998; Obata et al., 2004). Finally, the third constant term is defined as $k_3 = \beta - 1$.

References

An, H., Lin, W., 2002. Cerebral venous and arterial blood volumes can be estimated separately in humans using magnetic resonance imaging. Magn. Reson. Med. 48 (4), 583–588.

Ances, B.M., Greenberg, J.H., Detre, J.A., 2001. The effects of graded hypercapnia on the activation flow coupling response due to forepaw stimulation in alpha-chloralose anesthetized rats. Brain Res. 911 (1), 82–88.

Attwell, D., Iadecola, C., 2002. The neural basis of functional brain imaging signals. Trends Neurosci. 25 (12), 621–625.

Bakalova, R., Matsuura, T., Kanno, I., 2001. Frequency dependence of local cerebral blood flow induced by somatosensory hind paw stimulation in rat under normo- and hypercapnia. Jpn. J. Physiol. 51 (2), 201–208.

Bentourkia, M., Bol, A., Ivanoiu, A., Labar, D., Sibomana, M., Coppens, A., Michel, C., Cosnard, G., De Volder, A.G., 2000. Comparison of regional cerebral blood flow and glucose metabolism in the normal brain: effect of aging. J. Neurol. Sci. 181 (1–2), 19–28.

Buckner, R.L., Snyder, A.Z., Sanders, A.L., Raichle, M.E., Morris, J.C., 2000. Functional brain imaging of young, nondemented, and demented older adults. J. Cogn. Neurosci. 12 (Suppl. 2), 24–34.

Buxton, R.B., 2002. Introduction to Functional Magnetic Resonance Imaging. Cambridge University Press, Cambridge.

Buxton, R.B., Miller, K.L., Wong, E.C., Frank, L.R., 1998a. BOLD Signal Dynamics: The balloon model with viscoelastic effects. Proceedings of the Proc. 6th Annual Meeting ISMRM, Sydney, pp. 1401.

Buxton, R.B., Wong, E.C., Frank, L.R., 1998b. Dynamics of blood flow and oxygenation changes during brain activation: the balloon model. Magn. Reson. Med. 39, 855–864.

Cohen, E.R., Ugurbil, K., Kim, S.G., 2002. Effect of basal conditions on the magnitude and dynamics of the blood oxygenation level-dependent fMRI response. J. Cereb. Blood Flow Metab. 22 (9), 1042–1053.

D'Esposito, M., Deouell, L.Y., Gazzaley, A., 2003. Alterations in the BOLD fMRI signal with ageing and disease: a challenge for neuroimaging. Nat. Rev., Neurosci. 4 (11), 863–872.

D'Esposito, M., Zarahn, E., Aguirre, G.K., Rypma, B., 1999. The effect of normal aging on the coupling of neural activity to the BOLD hemodynamic response. NeuroImage 10, 6–14.

Davis, M.J., Gore, R.W., 1989. Length–tension relationship of vascular smooth muscle in single arterioles. Am. J. Physiol. 256 (3 Pt. 2), H630–H640.

Davis, M.J., Hill, M.A., 1999. Signaling mechanisms underlying the vascular myogenic response. Physiol. Rev. 79 (2), 387–423.

Davis, T.L., Kwong, K.K., Weisskoff, R.M., Rosen, B.R., 1998. Calibrated functional MRI: mapping the dynamics of oxidative metabolism. Proc. Natl. Acad. Sci. U. S. A. 95, 1834–1839.

Friston, K.J., 2002. Bayesian estimation of dynamical systems: an application to fMRI. NeuroImage 16 (2), 513–530.

Friston, K.J., Mechelli, A., Turner, R., Price, C.J., 2000. Nonlinear responses in fMRI: the balloon model, volterra kernels, and other hemodynamics. NeuroImage 12, 466–477.

Friston, K.J., Harrison, L., Penny, W., 2003. Dynamic causal modelling. NeuroImage 19 (4), 1273–1302.

Fung, Y., 1993. Biomechanics: Mechanical Properties of Living Tissues. Springer-Verlag, New York.

Fung, Y., 1994. A first Course in Continuum Mechanics. Prentice Hall, New Jersey.

Fung, Y.C., 1997. Biomechanics: Circulation. Springer-Verlag, New York.

Grubb, R.L., Raichle, M.E., Eichling, J.O., Ter-Pogossian, M.M., 1974. The effects of changes in $PaCO_2$ on cerebral blood volume, blood flow, and vascular mean transit time. Stroke 5, 630–639.

Hajdu, M.A., Heistad, D.D., Siems, J.E., Baumbach, G.L., 1990. Effects of aging on mechanics and composition of cerebral arterioles in rats. Circ. Res. 66 (6), 1747–1754.

Handwerker, D.A., Ollinger, J.M., D'Esposito, M., 2004. Variation of BOLD hemodynamic responses across subjects and brain regions and their effects on statistical analyses. NeuroImage 21 (4), 1639–1651.

Hoge, R.D., Atkinson, J., Gill, B., Crelier, G.R., Marrett, S., Pike, G.B., 1999. Linear coupling between cerebral blood flow and oxygen consumption in activated human cortex. Proc. Natl. Acad. Sci. U. S. A. 96 (16), 9403–9408.

Iadecola, C., 2004. Neurovascular regulation in the normal brain and in Alzheimer's disease. Nat. Rev., Neurosci. 5 (5), 347–360.

Irikura, K., Maynard, K.I., Moskowitz, M.A., 1994. Importance of nitric oxide synthase inhibition to the attenuated vascular responses induced by topical L-nitroarginine during vibrissal stimulation. J. Cereb. Blood Flow Metab. 14 (1), 45–48.

Ito, H., Kanno, I., Ibaraki, M., Hatazawa, J., Miura, S., 2003. Changes in human cerebral blood flow and cerebral blood volume during hypercapnia and hypocapnia measured by positron emission tomography. J. Cereb. Blood Flow Metab. 23 (6), 665–670.

Kashikura, K., Kershaw, J., Kashikura, A., Zhang, X., Matsuura, T., Kanno, I., 2001. Hyperoxia modified activation-induced blood oxygenation level-dependent response of human visual cortex (V1): an event-related functional magnetic resonance imaging study. Neurosci. Lett. 299 (1–2), 53–56.

Kastrup, A., Kruger, G., Neumann-Haefelin, T., Glover, G.H., Moseley, M.E., 2002. Changes of cerebral blood flow, oxygenation, and oxidative metabolism during graded motor activation. NeuroImage 15 (1), 74–82.

Kemna, L.J., Posse, S., 2001. Effect of respiratory CO(2) changes on the temporal dynamics of the hemodynamic response in functional MR imaging. NeuroImage 14 (3), 642–649.

Lash, J.M., Bohlen, H.G., Waite, L., 1991. Mechanical characteristics and active tension generation in rat intestinal arterioles. Am. J. Physiol. 260 (5 Pt. 2), H1561–H1574.

Leenders, K.L., et al., 1990. Cerebral blood flow, blood volume and oxygen utilization: normal values and effect of age. Brain 113, 27–47.

Li, D., Wang, Y., Waight, D.J., 1998. Blood oxygen saturation assessment in vivo using T2* estimation. Magn. Reson. Med. 39 (5), 685–690.

Logothetis, N.K., Wandell, B.A., 2004. Interpreting the BOLD signal. Annu. Rev. Physiol. 66, 735–769.

Mandeville, J.B., Marota, J.J.A., Ayata, C., Zaharchuk, G., Moskowitz, M.A., Rosen, B.R., Weisskoff, R.M., 1999. Evidence of a cerebrovascular postarteriole windkessel with delayed compliance. J. Cereb. Blood Flow Metab. 19 (6), 679–689.

Marchal, G., Rioux, P., Petit-Taboue, M.-C., Sette, G., Travere, J.-M., LePoec, C., Courtheoux, P., Derlon, J.-M., Baron, J.-C., 1992. Regional cerebral oxygen consumption, blood flow, and blood volume in healthy human aging. Arch. Neurol. 49, 1013–1020.

Martin, A.J., Friston, K.J., Colebatch, J.G., Frackowiak, R.S., 1991. Decreases in regional cerebral blood flow with normal aging. J. Cereb. Blood Flow Metab. 11 (4), 684–689.

Martinez-Lemus, L.A., Wu, X., Wilson, E., Hill, M.A., Davis, G.E., Davis, M.J., Meininger, G.A., 2003. Integrins as unique receptors for vascular control. J. Vasc. Res. 40 (3), 211–233.

Matsuura, T., Fujita, H., Kashikura, K., Kanno, I., 2000a. Evoked local cerebral blood flow induced by somatosensory stimulation is proportional to the baseline flow. Neurosci. Res. 38 (4), 341–348.

Matsuura, T., Fujita, H., Kashikura, K., Kanno, I., 2000b. Modulation of evoked cerebral blood flow under excessive blood supply and hyperoxic conditions. Jpn. J. Physiol. 50 (1), 115–123.

Matsuura, T., Kashikura, K., Kanno, I., 2001. Hemodynamics of local cerebral blood flow induced by somatosensory stimulation under normoxia and hyperoxia in rats. Comp. Biochem. Physiol., A: Mol. Integr. Physiol. 129 (2–3), 363–372.

Mayhew, J.E., Askew, S., Zheng, Y., Porrill, J., Westby, G.W., Redgrave, P., Rector, D.M., Harper, R.M., 1996. Cerebral vasomotion: a 0.1-Hz oscillation in reflected light imaging of neural activity. NeuroImage 4 (3 Pt. 1), 183–193.

Mehagnoul-Schipper, D.J., van der Kallen, B.F., Colier, W.N., van der Sluijs, M.C., van Erning, L.J., Thijssen, H.O., Oeseburg, B., Hoefnagels, W.H., Jansen, R.W., 2002. Simultaneous measurements of cerebral oxygenation changes during brain activation by near-infrared spectroscopy and functional magnetic resonance imaging in healthy young and elderly subjects. Hum. Brain Mapp. 16 (1), 14–23.

Mildner, T., Norris, D.G., Schwarzbauer, C., Wiggins, C.J., 2001. A qualitative test of the balloon model for BOLD-based MR signal changes at 3T. Magn. Reson. Med. 46, 891–899.

Miller, K.L., Luh, W.M., Liu, T.T., Martinez, A., Obata, T., Wong, E.C., Frank, L.R., Buxton, R.B., 2001. Nonlinear temporal dynamics of the cerebral blood flow response. Hum. Brain Mapp. 13 (1), 1–12.

Murray, K.J., 1990. Cyclic AMP and mechanisms of vasodilation. Pharmacol. Ther. 47 (3), 329–345.

Obata, T., Liu, T.T., Miller, K.L., Luh, W.M., Wong, E.C., Frank, L.R., Buxton, R.B., 2004. Discrepancies between BOLD and flow dynamics in primary and supplementary motor areas: application of the balloon model to the interpretation of BOLD transients. NeuroImage 21 (1), 144–153.

Panczel, G., Daffertshofer, M., Ries, S., Spiegel, D., Hennerici, M., 1999. Age and stimulus dependency of visually evoked cerebral blood flow responses. Stroke 30 (3), 619–623.

Pantano, P., Baron, J.C., Lebrun-Grandie, P., Duquesnoy, N., Bousser, M.G., Comar, D., 1984. Regional cerebral blood flow and oxygen consumption in human aging. Stroke 15 (4), 635–641.

Richter, W., Richter, M., 2003. The shape of the fMRI BOLD response in children and adults changes systematically with age. NeuroImage 20 (2), 1122–1131.

Riddle, D.R., Sonntag, W.E., Lichtenwalner, R.J., 2003. Microvascular plasticity in aging. Ageing Res. Rev. 2 (2), 149–168.

Rosengarten, B., Spiller, A., Aldinger, C., Kaps, M., 2003. Control system analysis of visually evoked blood flow regulation in humans under normocapnia and hypercapnia. Eur. J. Ultrasound 16 (3), 169–175.

Rostrup, E., Law, I., Pott, F., Ide, K., Knudsen, G.M., 2002. Cerebral hemodynamics measured with simultaneous PET and near-infrared spectroscopy in humans. Brain Res. 954 (2), 183–193.

Schroeter, M.L., Zysset, S., Kruggel, F., von Cramon, D.Y., 2003. Age dependency of the hemodynamic response as measured by functional near-infrared spectroscopy. NeuroImage 19 (3), 555–564.

Silva, A.C., Iadecola, C., Kim, S.-G., 1999. The Dependence of BOLD and CBF Changes on the CBF Baseline During Somatsensory Simulation. Proceedings of the Seventh ISMRM Scientific Meeting, Philadelphia, PA, pp. 1736.

Silvennoinen, M.J., Clingman, C.S., Golay, X., Kauppinen, R.A., van Zijl, P.C., 2003. Comparison of the dependence of blood R2 and R2* on oxygen saturation at 1.5 and 4.7 Tesla. Magn. Reson. Med. 49 (1), 47–60.

Somlyo, A.P., Somlyo, A.V., 1994. Signal transduction and regulation in smooth muscle. Nature 372 (6503), 231–236.

Stewart, G.N., 1894. Researches on the circulation time in organs and on the influences which affect it: parts I–III. J. Physiol. (London) 15, 1–89.

Taoka, T., et al., 1998. Age correlation of the time lag in signal change on EPI-fMRI. J. Comput. Assist. Tomogr. 22 (4), 514–517.

Ursino, M., 1991. Mechanisms of cerebral blood flow regulation. Crit. Rev. Biomed. Eng. 18, 255–288.

West, G.A., Meno, J.R., Nguyen, T.S., Ngai, A.C., Simard, J.M., Winn, H.R., 2003. cGMP-dependent and not cAMP-dependent kinase is required for adenosine-induced dilation of intracerebral arterioles. J. Cardiovasc. Pharmacol. 41 (3), 444–451.

Wilson, H.R., 1999. Spikes, Decisions and Actions: Dynamical Foundations of Neuroscience. Oxford University Press, Oxford.

Yacoub, E., et al., 2001. Imaging brain function in humans at 7 Tesla. Magn. Reson. Med. 45 (4), 588–594.

Yang, J., Clark Jr., J.W., Bryan, R.M., Robertson, C., 2003a. The myogenic response in isolated rat cerebrovascular arteries: smooth muscle cell model. Med. Eng. Phys. 25 (8), 691–709.

Yang, J., Clark Jr., J.W., Bryan, R.M., Robertson, C.S., 2003b. The myogenic response in isolated rat cerebrovascular arteries: vessel model. Med. Eng. Phys. 25 (8), 711–717.

Zheng, Y., Martindale, J., Johnston, D., Jones, M., Berwick, J., Mayhew, J., 2002. A model of the hemodynamic response and oxygen delivery to brain. NeuroImage 16 (3 Pt. 1), 617–637.